9-2008

Active and Passive Imaging in the THz Spectral Region: Phenomenology, Dynamic Range, Modes, and Illumination

Douglas T. Petkie
Wright State University - Main Campus, dpetkie@yahoo.com

Corey Casto

Frank C. De Lucia

Steven R. Murrill

Brian Redman

See next page for additional authors

Active and passive imaging in the THz spectral region: phenomenology, dynamic range, modes, and illumination

Douglas T. Petkie,[1] Corey Casto,[2] Frank C. De Lucia,[2,*] Steven R. Murrill,[3] Brian Redman,[4] Richard L. Espinola,[5] Charmaine C. Franck,[6] Eddie L. Jacobs,[7] Steven T. Griffin,[7] Carl E. Halford,[7] Joe Reynolds,[5] Sean O'Brien,[8] and David Tofsted[8]

[1]*Department of Physics, Wright State University, Dayton, Ohio 45435, USA*
[2]*Department of Physics, Ohio State University, Columbus, Ohio 43210, USA*
[3]*Army Research Laboratory, Adelphi, Maryland 20783, USA*
[4]*Lockheed Martin Coherent Technologies, Louisville, Colorado 80027, USA*
[5]*Night Vision and Electronic Sensors Directorate, Fort Belvoir, Virginia 22060, USA*
[6]*CACI Technologies Incorporated, Fort Belvoir, Virginia 22060, USA*
[7]*Department of Electrical and Computer Engineering, University of Memphis, Memphis, Tennessee 38152, USA*
[8]*Army Research Laboratory, White Sands, New Mexico 88002, USA*
[*]*Corresponding author: fcd@mps.ohio-state.edu*

Received December 18, 2007; revised May 2, 2008; accepted June 6, 2008;
posted June 26, 2008 (Doc. ID 90381); published August 21, 2008

The useful compromise between resolution and penetration power of the submillimeter or terahertz (THz) spectral region has long made it attractive for a variety of imaging applications. However, many of the demonstrations of imaging in this spectral region have used strategically oriented targets, especially favorable concealment materials, proximate imaging geometries, etc. This paper reports the results of studies aimed at better understanding the phenomenology of targets, the impact of this phenomenology on various active and passive imaging strategies, and most importantly, the development of imaging strategies that do not require the aforementioned special circumstances. Particular attention is paid to the relationship between active and passive images, especially with respect to how they interact with the illumination- and detector-mode structures of various imaging scenarios. It is concluded that the very large dynamic range that can be obtained with active single-mode systems (including focal-plane arrays) can be used in system designs to overcome the deleterious effects that result from the dominance of specular reflections in single-mode active systems as well as to strategically orient targets to obtain recognition. This will aid in the development of a much more robust and generally useful imaging technology in this spectral region.

OCIS codes: 110.01110, 120.5630.

1. INTRODUCTION

For many years there has been considerable interest in the use of the spectral region that has variously been referred to as the millimeter, near millimeter, submillimeter, far infrared, or terahertz (THz) region for imaging [1–6]. Briefly put, much of this interest is because this spectral region represents a useful compromise between imaging resolution and atmospheric/obscurant penetration [7]. For the purposes of this discussion, we will refer to this region of the electromagnetic spectrum as the THz region. We will also adopt as the bounds of this region the oft-used 0.1–10 THz, but will focus primarily on the region centered on the atmospheric window at 640 GHz (0.64 THz).

Much of the recent activity and visibility of imaging here has been focused on the use of THz time-domain spectroscopy (THz-TDS) approaches used to make T-ray images. The first such images were obtained in transmission by Hu and Nuss, who used an *x-y* translation of targets such as leaves and packaged semiconductors within a pair of proximate off-axis paraboloids [8]. A number of other proximate near-field THz-TDS approaches have also been demonstrated [9–11].

However, the main thrust of this paper is on images of targets positioned at some distance (>1 m) that are imaged without a synchronous movement of the target. Some years ago we used a cooled bolometer and a raster scan of an 8 in. mirror to make a passive thermal image of the upper torso of a man [12]. Active images have also been considered [13–15], as have interferometric and synthetic aperture techniques [16,17].

Finally, there is often a rather ill-defined line between millimeter-wave and terahertz images, and we need to recognize, for completeness, the many impressive THz images in the literature at 94 GHz (0.094 THz) and below. These passive images typically make use of cold sky illumination [18].

Much of the effort to date has been on the development and demonstration of imaging technology. In this paper we are primarily concerned with the phenomenology of the scenarios with which potential imagers will have to interact and the nature of the images that result as a function of imaging strategy.

Because of the broad definition of the THz region, imaging systems will have widely varying performance characteristics. The focus of this work is centered on 640 GHz

but is generally representative of the region between perhaps 300 and 1000 GHz. We will show that, in this region, the phenomenology is related to the scale of the texture and surface roughness of targets relative to the imaging wavelength. As a result, images will scale in a more-complex fashion with wavelength, range, and optics size than would be inferred solely from diffraction considerations.

2. EXPERIMENT

A block diagram of the active imaging system used in this work is shown in Fig. 1. It is a raster-scanned single-pixel imager, whose images (and the phenomenology on which they are based) should be very similar to those that will be produced by focal plane array-based systems as they are developed for this spectral region.

The transmitter and receiver are combined with a beam splitter and coupled to a 30 cm diameter, 0.5 m focal length spherical mirror. As a result, the same diffraction-limited spot on the object is illuminated and viewed by the mode that is defined by the 30 cm mirror. For an object 1.5 m from the mirror, the illuminated spot width on the object at 640 GHz is ~0.25 cm.

Active imaging systems in this spectral region can have very high signal-to-noise (S/N) ratios and correspondingly large dynamic ranges. The frequency multiplier chains of the transmit and receive modules start with 13.3 and 13.4 GHz phase-lock oscillators, respectively, which are locked to the same 100 MHz crystal reference. Both are subsequently multiplied by ×48 in multiplier chains produced by Virginia Diodes, Inc. The resultant intermediate frequency (IF) is 4.8 GHz. The exit aperture transmit power of this system is ~1 mW and the receiver noise temperature is ~3000 K.

The bandwidth associated with the system is determined by its dwell time on a diffraction-limited spot; in our system this limit is set by mechanical considerations to ~0.01 s. The limit set by a desirable video frame rate for a focal-plane system would be similar. Thus, the minimum receiver bandwidth is ~100 Hz. If an illumination power P_I is confined to a bandwidth $\Delta\nu$, the illumination temperature T_I is

$$T_I = \frac{P_I}{k\Delta\nu}. \tag{1}$$

1 mW in a 100 Hz bandwidth corresponds to a temperature of $\sim 10^{18}$ K, more than 140 dB above the noise temperature of the receiver. An important feature of the system shown in Fig. 1 is that it makes use of a logarithmic IF amplifier to take advantage of this dynamic range. We will see below that many of the strategies that we will discuss to overcome some of the shortcomings of active imaging will make use of this large system margin. While we typically used 1 kHz video and 100 kHz rf bandwidths, inspection of the spectral purity of the received signal after it had been converted into the 4.8 GHz IF showed it to be under 100 Hz.

The labeled axes of many of the pictures in this paper provide the location in the final display matrix. This matrix is of the order 1000×1000 and is chosen to be 5–10 times finer than the matrix of the diffraction-limited pixels. In the vertical (the direction of the continuous scan), the pixel size is the same as the display scale (and each of these pixels is the result of many samples—i.e., we oversample in the vertical direction as we scan). The horizontal separation between scan lines or pixels is set by an operator choice in the horizontal step size. Typically, the horizontal steps (pixels) are separated by 2 or 3 times the vertical pixels in the display matrix, while still less than the diffraction-limited spot size. To produce the final image, the missing horizontal display pixels are obtained by

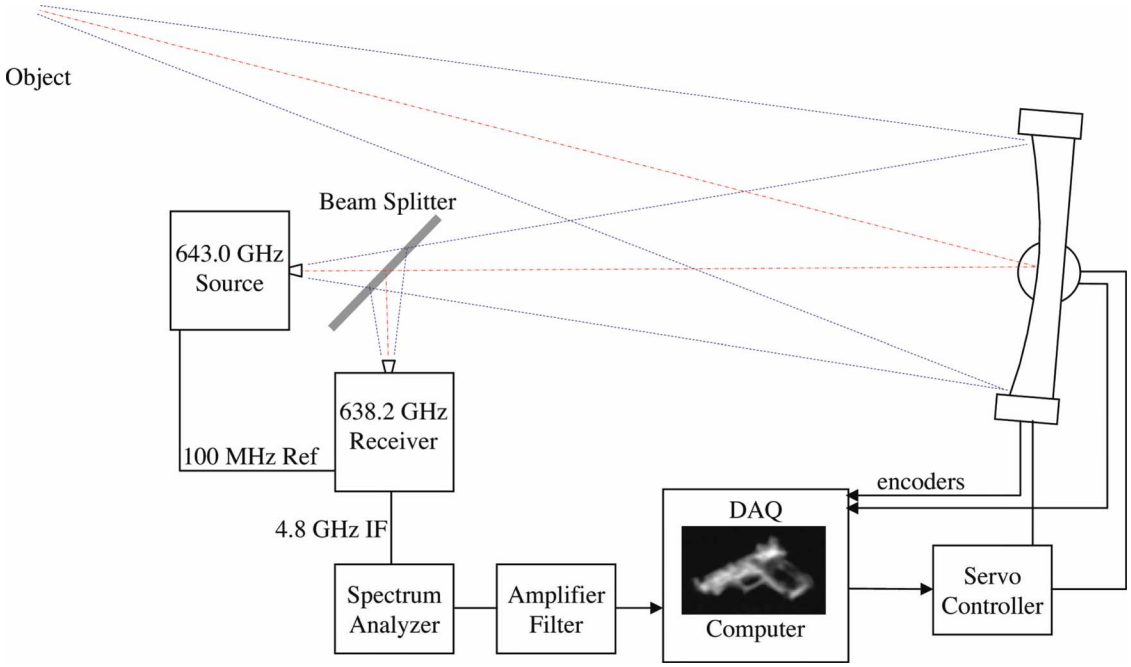

Fig. 1. (Color online) Block diagram of the 640 GHz active imaging system.

a linear interpolation between their horizontal neighbors such that the horizontal and vertical dimensions of each pixel are equal.

The passive images, shown below in Fig. 6, were made with the same heterodyne receiver and optics as the active system described above, with two modifications. The beam splitter was replaced with a mirror so that all of the power collected was directed to the receiver. Additionally, the full 10 GHz bandwidth of the receiver was used to maximize the collection of the black body radiation. In this case, both of the image sidebands were collected, so the effective bandwidth was 20 GHz.

We have previously described the passive system that produced the image shown in Fig. 2 [12]. This system was assembled on short notice from existing spectroscopic components to provide an example of a submillimeter image for a workshop. Briefly, an 8 in. mirror was used to raster scan the object by the use of positions on a mirror mount. The detector was a ^{3}He silicon bolometer, bandpass limited to ~200–1000 GHz, with a noise-equivalent power (NEP) of $\sim 2\times 10^{-15}$ W/Hz$^{1/2}$. With a 30 ms time constant, the S/N ratio of the system was considerably greater than the gray scale capabilities of the system.

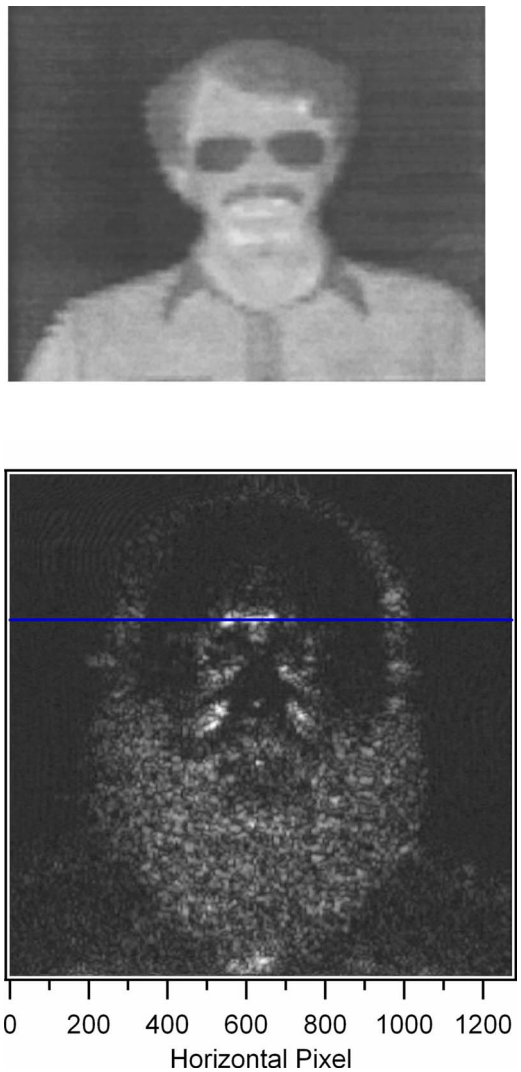

Fig. 2. (Color online) Passive image (upper) and active image (lower). Both are at $\lambda \sim 0.5$ mm (600 GHz) and have similar, diffraction-limited spot sizes of ~5 mm on the target image. However, the upper image is of a clean-shaven individual with a mustache, whereas the lower image is of a bald individual with a full beard.

3. ACTIVE VERSUS PASSIVE IMAGING

A. Some Introductory Remarks

We would like to begin by making some general observations about the relationship between active and passive imaging in the THz region and discussing the nature of the images that each produces. The upper image in Fig. 2 is a passive image that we made some time ago [12] with the bolometer-based passive system described in Section 2. In this image, the slightly warmer areas of the face associated with blood flow in the lips and throat areas are readily observable, as are the extra layers of cloth in the button and collar regions of the shirt. The glasses appear dark, because they are cooler than body temperature or because they reflect the cooler room temperature. In addition to the emissive contribution to this image, the signal also includes a reflective component of the illumination from the surrounding room. However, this has little impact on the observed image because of the uniformity of this room temperature illumination. A similar observation can be made about outdoor images because at 640 GHz, atmospheric absorption and emission preclude the very strong sky illumination that dominates most 94 GHz images. This lack of sky illumination places more stringent sensitivity limits on passive 640 GHz systems.

The active figure shown in the lower panel is much more complex and much less pretty. To provide a numerical reference, the linear signal level taken along the blue line in the active image is plotted in Fig. 3. There are two notable features in this image. First, because even at 640 GHz the roughness of skin is still small in comparison to a wavelength, the reflections are largely specular, and only those parts of the image that are near perpendicular return a significant signal. On the other hand, the hair being on the order of $\lambda/4$ (18–180 μm) provides a strong return to the imager. The histogram adjustment shown in Fig. 4 of the image in Fig. 2 highlights certain specular regions, such as the area around the eyes. Thus, the active image is very different from typical optical images, which are dominated by diffuse reflection. Similar observations have been reported at 220 GHz [15]. They are also very different from the passive image shown in the upper panel of Fig. 2, which is more a measure of the thermal emissivity and physical temperature, independent of the angle between the observer and the emitting surface.

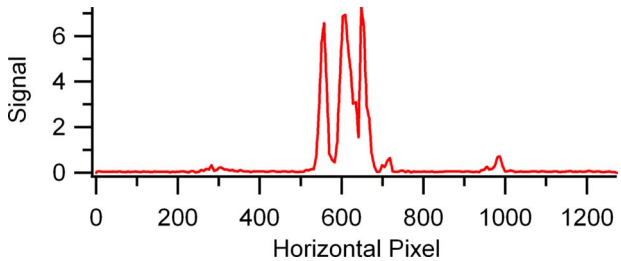

Fig. 3. (Color online) Signal intensity taken along the horizontal line in the active image of Fig. 2.

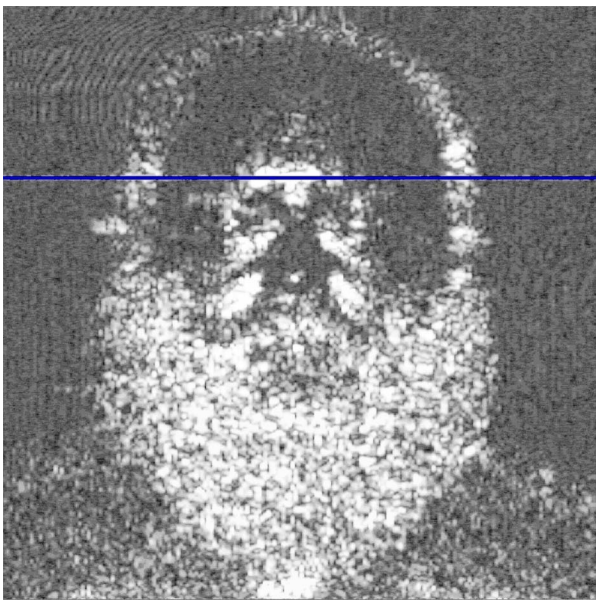

Fig. 4. (Color online) Histogram alteration of active image (gamma correction and stretching).

Fig. 5. (Color online) 94 GHz radiometer image taken outdoors with cold sky illumination (courtesy of R. Appleby).

B. Angular Diversity and Modes in Active Imaging

Much of the difference between the active and passive images shown in Fig. 2 results from the fact that the imager used to make the active image confines all of its illumination to a single mode, and the receiver observes this same mode.

If a perpendicular specular target is illuminated with a copropagated, single-mode system, all of the illumination power is returned to that mode. If a diffuse target is illuminated, the power from the illuminator is distributed into $\sim(ss/\lambda)^2=N_{AD}$ modes, where ss is the diffraction spot width resolvable by the imager on the target. For the system described in Section 2, $ss\sim 2.5$ mm and the number of modes ~ 25.

Alternatively, if one wants to illuminate a target with full angular diversity, in the context of the system optics with a collecting aperture D and range to the target r, then $N_{AD}\sim(r/D)^2$, also 25. For an active system, this would require a corresponding increase in power, or, if the illumination power is divided among these modes, a corresponding reduction in the excitation temperature of these modes. However, as noted above, if all of the power of even a 1 mW illuminator is concentrated in a single mode, the illumination temperature is very high, and a significant reduction in this temperature would be practical in most cases. In comparison, the noise power associated with a single-mode receiver is

$$P_N = kT_N(Bb)^{1/2}, \tag{2}$$

where T_N is the noise temperature of the receiver, b is the optical bandwidth (typically the IF bandwidth) of the system, and B is the bandwidth associated with the system integration time.

As we have noted above, for a 1 mW, single-mode illuminator with $b=100$ Hz, $T_{\text{eff}}\sim 10^{18}$ K. This is a very large number because the amount of thermal noise in this spectral region in a narrow bandwidth is very small. For example, if we have a receiver whose noise temperature is 3000 K, and if we use a 100 Hz bandwidth so that our source power fits within the 100 Hz width, the dynamic range (assuming no system saturation) is $\sim 3\times 10^{14}$. Viewed alternatively via Eq. (2), for these parameters $P_N\sim 4\times 10^{-18}$, and the 1 mW source again provides a dynamic range of $\sim 3\times 10^{14}$.

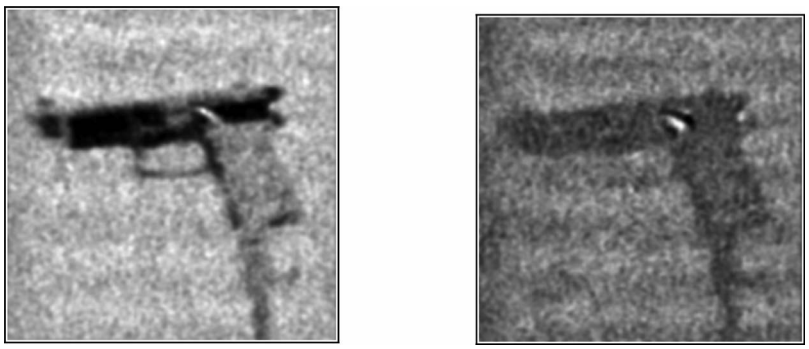

Fig. 6. 640 GHz passive image of a gun in front of a warm background (right) and an image of the same gun illuminated by a cold illuminator that fills $\sim 15°$ (left).

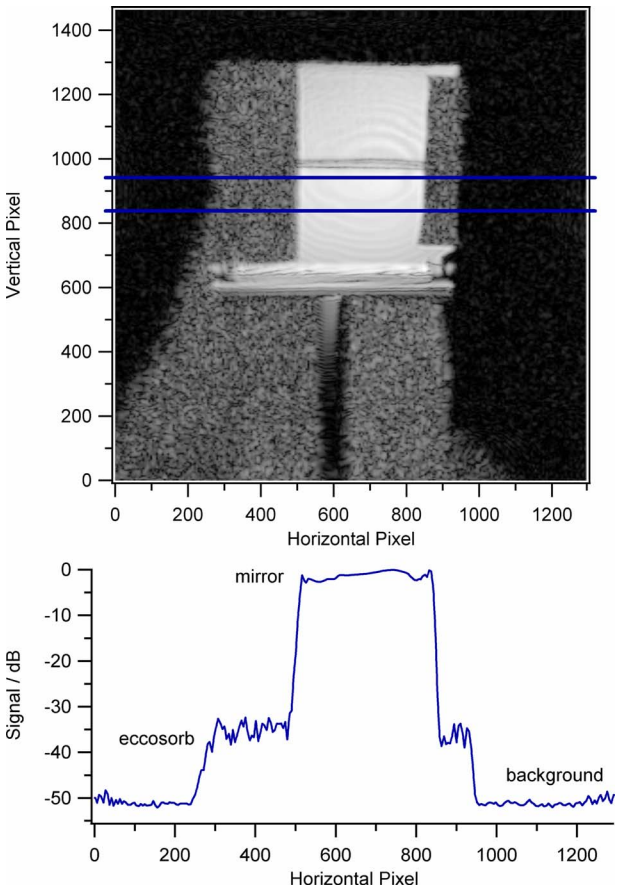

Fig. 7. (Color online) 640 GHz active image of a mirror at normal incidence. The left and right sides of the mirror are covered by Eccosorb, and the top half is covered by a thin scarf. Below the image is a quantitative plot of the averaged signal intensities between the two horizontal lines in the image. The image was recorded and displayed on a logarithmic scale because of its large dynamic range. The T-shaped object in the lower half of the image is a support structure.

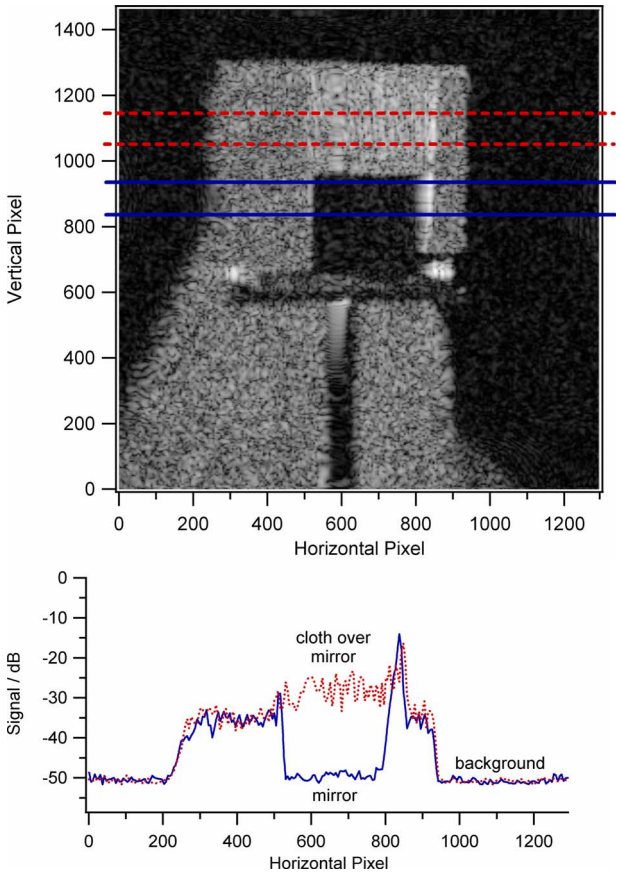

Fig. 8. (Color online) 640 GHz active image of the same system as shown in Fig. 7, but at an incidence angle of 10° to the normal. Below the image is a quantitative plot (solid curve) of the signal intensities between the solid lines in the images. Below the image is a quantitative plot (dotted curve) of the signal intensities between the dotted lines in the images.

C. Angular Diversity and Modes in Passive Imaging

Passive imaging is often considered to include all systems that do not use a narrowband, coherent illuminator such as an electronic THz source or a laser. The best known systems are similar to those used to produce the passive image shown in Fig. 5. In this system, a 94 GHz radiometer was used to observe a subject outdoors. The cold sky radiance, which is the sum of the 3 K cosmic background radiance transmitted through the atmospheric air mass and the thermal radiance from the gray-body atmosphere along a given line of sight, provides effective sky temperatures that range from about 60 K near the zenith to near ambient at the horizon under clear conditions at 94 GHz [19,20]. The dependence of this effective temperature with the zenith angle is strongly affected by the vertical distribution of atmospheric humidity. This image looks very different from the THz passive image shown in Fig. 2 because it is dominated by a very bright, cold illuminator that fills a fraction of the modes that surround the target and because the knife is oriented to optimally reflect the cold sky.

Figure 6 shows two passive images taken indoors with the 640 GHz heterodyne radiometer described in Section 2. The image on the right shows a gun in front of a warm background. Because this image was made indoors, all of the modes associated with the illumination angles that are reflected into the detection mode of the imager from the variously angled surfaces of the gun have the same (room) temperature. If the metal of the gun were a perfect reflector, its temperature would not contribute to the contrast in the image. In this case, even those parts of the gun whose emissivities are equal to 1 do not contribute contrast because the gun is also at room temperature. This image is best thought of as a shadowgram with two temperatures: the background temperature, which might come from a body, and the constant room temperature, which comes from the many, but equal in temperature, illumination modes of the surroundings.

The image on the left shows considerably more contrast because the cold illuminator only fills a fraction of the solid illumination angle. The dark regions along the gun barrel are properly oriented to reflect the cold illumination, whereas the rest of the gun reflects the temperature that is common to the gun and the rest of the room/enclosure. Thus, at 650 GHz (either indoors or outdoors) careful consideration must be given to sources of temperature differential that the target can in turn translate into an image. This is significantly different from the 94 GHz outdoors case.

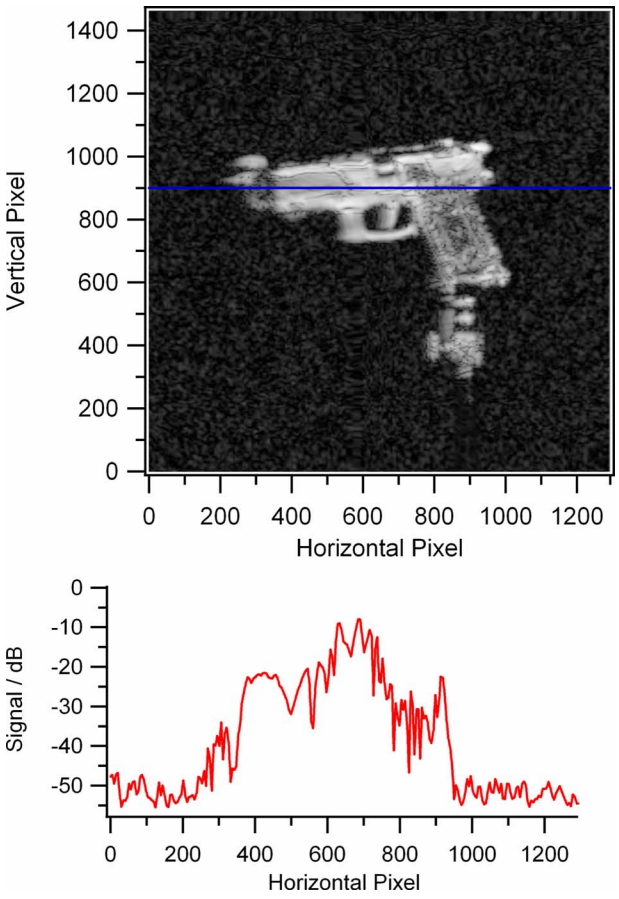

Fig. 9. (Color online) Active image of a toy gun recorded and displayed on a logarithmic scale (upper). The quantitative reflection (relative to a normal specular reflection) along the horizontal line is shown in the lower panel.

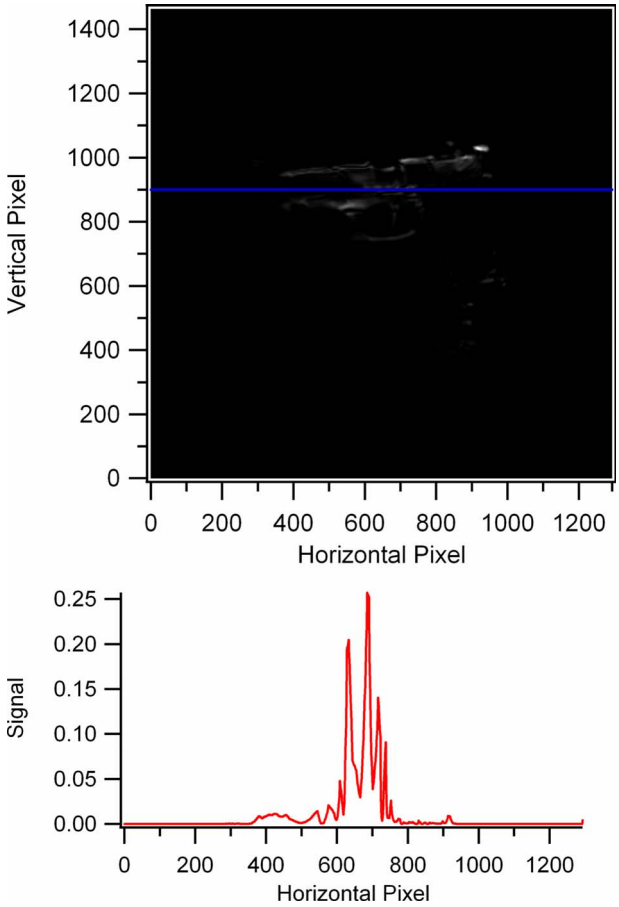

Fig. 10. (Color online) Active image displayed on a linear scale of the same object displayed on a log scale in Fig. 9.

Finally, let us consider the magnitude of this thermal signal. For a thermal source at a temperature of T_I, the thermal power in the bandwidth b is

$$P_I = kT_I b, \tag{3}$$

and combined with Eq. (2), the signal to noise becomes

$$S/N = (T_I/T_N)(b/B)^{1/2}, \tag{4}$$

or for a S/N=1,

$$T_I = T_N(B/b)^{1/2}. \tag{5}$$

For numbers typical of a heterodyne system at 600 GHz (T_N=3000 K; B=100 Hz; $b=10^{10}$ Hz), T_I=0.3 K. If a target has a temperature differential of 30 K, this will provide a dynamic range of 100. This is a typical result for a passive heterodyne receiver at 640 GHz.

D. Angular Diversity and the Dynamic Range of Illumination

In the sections above, we have found for the most straightforward systems that the nature of the images and the signal margins of active and passive systems are very different. In this section, we would like to explore the reasons for this and see if it is possible to develop a hybrid approach to imaging that represents a compromise between the system margins associated with active systems and the perceived superior image quality and lack of special target angular alignments for true (i.e., non-sky illuminated) passive systems.

In order to be quantitative, let us consider the geometrical factors of the system shown in Fig. 1 that place constraints on the dynamic range of the signal from objects in the image plane. This system can be used in either active or passive mode, according to whether the spot illuminator of Fig. 1 or some other illuminator is used. The system has a 30 cm diameter imaging mirror positioned at a distance of 145 cm from the target. The upper limit of the return signal assumes a flat metallic target oriented perpendicularly to the direction of propagation, i.e., specular reflection. The lower limit assumes a rough dielectric, or Lambertian, surface with a ~5% reflection coefficient due to the dielectric mismatch. The hemisphere centered on the target of radius 145 cm has a total area of ~132000 cm^2. Thus the fraction of power collected by the aperture of the imaging mirror from an object that uniformly emitted (or scattered by a diffuse surface) into the hemisphere is approximately 0.005. Assuming the 5% reflectivity for active imaging, the return signal would be down by −36 dB relative to specular reflection. If the normal (perpendicular) of a specular object is tilted away from the direction of propagation by more than the geometrical factor of $\boldsymbol{l}/2D$ (5.7° for this configuration), the resulting return signal will typically be lower than −36 dB since the system will be illuminating an object beyond the

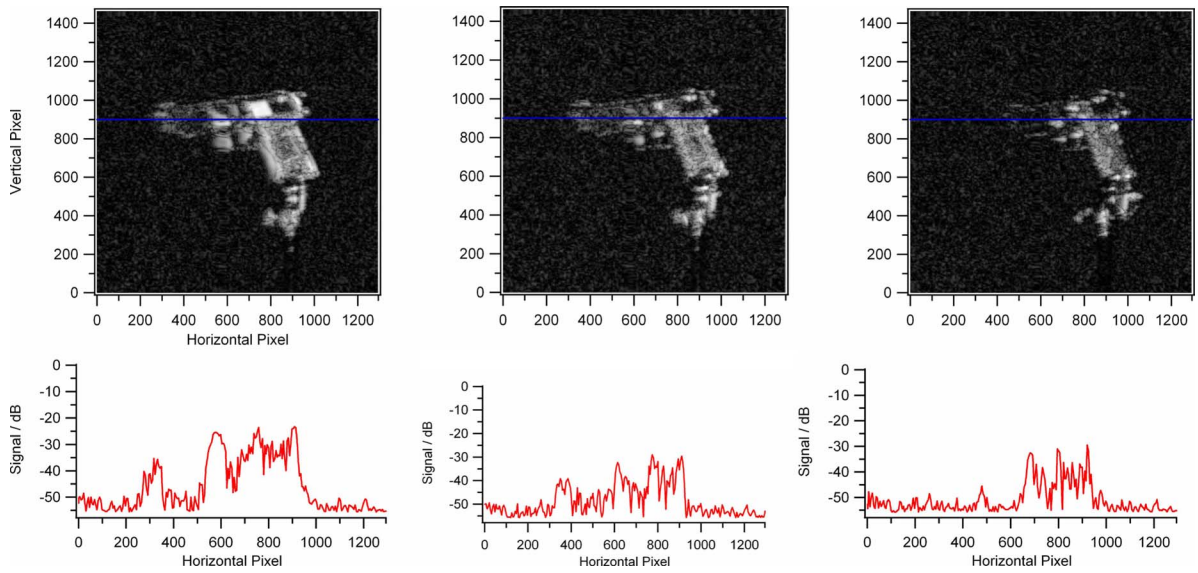

Fig. 11. (Color online) Logarithmic images of the toy gun rotated 10°, 20°, and 40° relative to the normal (left to right in the upper panels). Logarithmic intensities along the horizontal line in the upper panels of the toy gun rotated 10°, 20°, and 40° relative to the normal specular reflection (left to right in the lower panels).

image plane. Depending on the potential complex topology of the object in the image plane, the return signal will be confined to this dynamic range. This system would be equivalent to a standoff imaging system operating at a distance of 5 m with a 1 m aperture.

Let us consider the images from a well-characterized target shown in Figs. 7 and 8. The return from the center of the mirror in Fig. 7 corresponds to the case for which all of the power in the source mode is returned to the single mode of the receiver, i.e., specular reflection. Ignoring optical losses, this corresponds to the single-mode active case discussed quantitatively in Section 3.B. On each side of the mirror, the return by Eccosorb, considered a diffuse reflector, is reduced by 35 dB. The background Eccosorb that is beyond the image plane is reduced by 50 dB. For the 10° rotated target shown in Fig. 8, the return from the mirror is reduced by about 50 dB. It is important to note that the system noise is much lower than the signals displayed in these images and plots. Thus, the signal return from the 10° mirror is a real signal and represents the power that illuminated the mirror was redirected toward a new background by the inclined mirror, scattered by this background, and a small amount returned to the receiver mode by the mirror. Since the scattering backgrounds to the right of the mirror and behind the mirror are both Eccosorb at approximately the same distance from the mirror, the two returns are similar in intensity. The good agreement between the above calculations and measured returns is consistent with our observation that dielectric scattering media all have very similar reflectivity.

The image of Fig. 8 is interesting in that it shows that there is no obvious difference between the return from the Eccosorb (on the sides of the mirror) and the excess portion of the thin cloth that drapes behind and below the mirror after it was used to cover the upper half of the mirror. However, the return from the area covered by the cloth at the top of the mirror is greater by about 5 dB, presumably due to the additional power that passed through the cloth, which was then reflected by the mirror towards the background on the right, but which was rescattered by the cloth toward the imaging optics.

Now let us reconsider the active image shown in Fig. 2. This more controlled experiment with the mirror and the Eccosorb shows that the off-axis skin returned little target information for the same reasons that the rotated mirror returned little signal: the specular reflection out of the imaging collection mode by the nonnormal skin.

4. ALTERNATIVES TO SINGLE-MODE ACTIVE ILLUMINATION

We have seen that in a single-mode active system there can be a very large margin in S/N ratio. Here we explore the use of this margin in exchange for angular diversity, both for the purpose of removing the need for carefully chosen target orientations and also to provide a fuller interrogation of target signatures in systems dominated by specular reflection.

To achieve total diversity of angular illumination, the illuminator power must be divided into an appropriate number of modes, N_{AD}. The number of modes (approximately 25 in our example above), will grow rapidly for cases where the target range grows more rapidly than the aperture of the imaging optics. The temperature of illumination in each of the modes into which the illuminator power is scattered by the diffuse target is given by

$$T_I = \left(\frac{P_I}{k\Delta\nu}\right)\left(\frac{\lambda}{ss}\right)^2 = \left(\frac{P_I}{k\Delta\nu}\right)\left(\frac{D}{r}\right)^2, \tag{6}$$

where $(P_I/k\Delta\nu)$ is the power in a single mode and $(\lambda/ss)^2$ or $(D/r)^2$ accounts for all of the modes in the hemisphere illuminated by the diffuse scatterer.

However, this relationship assumes an optical system that still focuses all of its power on the single diffraction-limited spot that is being observed by the receiver. This

would be both difficult to implement and inconsistent with the spirit of a focal plane array-based system.

A. Flood Light Illumination

Instead of focused illumination, let us consider a target of scale l that we want to floodlight (i.e., simultaneously illuminate the complete target). The number of modes that we must fill is then $\sim(l/\lambda)^2$, and the temperature per mode becomes

$$T_I \approx \left(\frac{P_I}{k\Delta\nu}\right)\left(\frac{\lambda}{l}\right)^2. \tag{7}$$

This is a consequence of the single-mode antenna theorem, which states that the solid angle associated with a diffraction-limited single mode from an area A is given by

$$\Omega_{\text{blackbody mode}} = \frac{\lambda^2}{A}. \tag{8}$$

If one assumes $l=1$ m and $\lambda=0.5$ mm, the reduction factor becomes 4×10^6, and the illumination temperature in our narrow band (100 Hz) example is reduced to $\sim2\times10^{11}$ K. This is still very large in comparison to the receiver noise temperature.

B. The Indirect Lighting Limit

While in principle it is possible to strategically illuminate a target to provide angular diversity, a rather specific and large illuminator geometry may be required. Another limit would be to consider the illumination of an entire room or urban canyon of scale l and wall reflectivity R. The target then would reflect this indirect lighting in analogy to the common use of indirect lighting in the visible region. In this case the illumination temperature would be

$$T_I \approx R\left(\frac{P_I}{k\Delta\nu}\right)\left(\frac{\lambda}{l}\right)^2. \tag{9}$$

If we assume a reflectivity $R_w\sim0.1$ and $l=100$ m, in the case of a 1 mW illuminator power and 100 Hz bandwidth, $T_I\sim2.5\times10^6$ K.

In comparison to a receiver with a noise temperature of 3000 K, this is also a very large temperature. While this indirect lighting limit may seem to be very inefficient, this is often the nature of useful lighting. In the optical regime, we light an entire room; we do not observe it with a diffraction-limited laser beam. While THz photons are more difficult to obtain than optical photons, narrowband heterodyne receivers are correspondingly more sensitive.

5. RESULTS

In this section we will provide some specific results for two objects of interest, a toy gun and a metal cylinder. These images illustrate some of the issues raised above, especially the large variations in signal levels that are returned from different parts of these objects as a function of observation and illumination angle.

Figure 9 shows a logarithmic image of a toy gun at near, but not at exact, normal incidence. The signal intensity measured along the blue line in the image is plotted in the lower panel. The largest signal return is down by ~10 dB relative to a normal specular reflection. While the signal levels from other parts of the target are down by as much as 35 dB, this logarithmic image still provides significant identification information. The signal level on either side of the gun is provided by the clutter associated with the Eccosorb background; the system noise shown in this figure is negligible.

In contrast, the linear image of the same target shown in Fig. 10 is dominated by a few glints. The largest of these (located at pixel $V\sim1000$, $H\sim900$) produced a return nearly equal to that of a normal specular reflector. If the gun had been perfectly posed, the large flat areas of this particular gun would have returned signals at a similar level and would have made its identification in the linear picture straightforward as well. These figures illustrate a rather general effect and show why THz images are often shown with strategically chosen target orientations.

Figure 11 extends this series to include logarithmic images of the gun at 10°, 20°, and 40°. With the logarithmic signal processing and display, even at these large angles the gun is readily identifiable. Again, all of the signal that surrounds the gun is clutter from the background.

Figure 12 shows a similar logarithmic image of a metallic cylinder. Because of the well-defined geometry of this target, the bright stripe down the middle of the cyl-

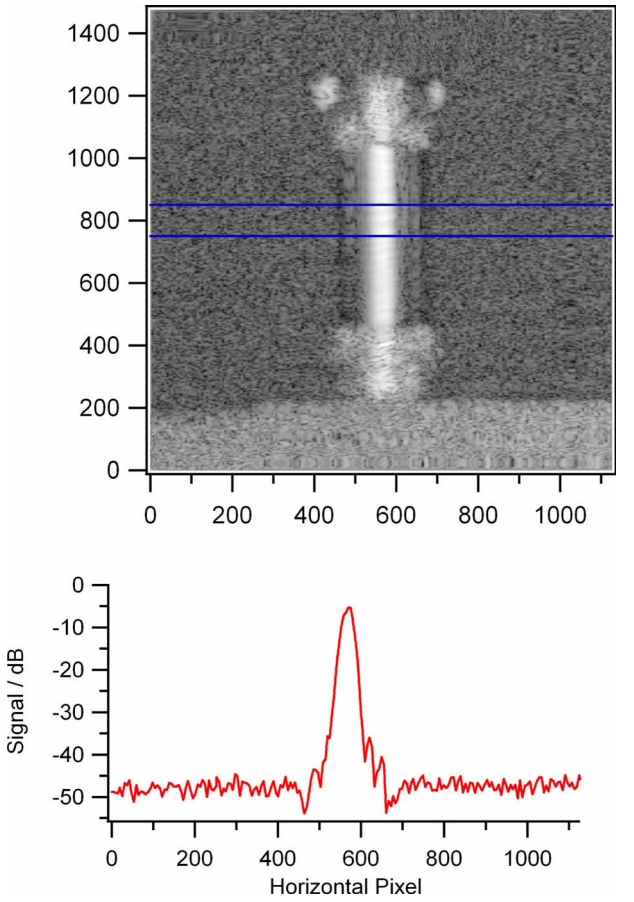

Fig. 12. (Color online) Active image of a 4.25 cm diameter metallic cylinder with end caps recorded and displayed on a logarithmic scale (upper). The average reflected signal between the horizontal lines in the figure is also shown (lower).

inder can be identified with a specular reflection from the normal part of the cylinder. The return from the nonnormal parts of the cylinder contain contributions due to multiple reflections between the cylinder and its immediate background. The geometry of this image is equivalent to a continuous rotation of the plane mirror shown in Figs. 7 and 8.

6. CONCLUSIONS

From this work, we can draw a number of conclusions that are of importance in the selection of imaging strategies at 640 GHz and the spectral regions that extend by perhaps a factor of 2 in either direction.

1. Active imaging systems with narrowband heterodyne receivers can have very large dynamic ranges, even with very modest illumination power. 1 mW in a 100 Hz bandwidth corresponds to $\sim 10^{18}$ K.

2. Because the wavelength of radiation at 640 GHz is intermediate between the optical (where most images are dominated by diffuse reflection because the surface texture of targets is typically larger than the wave length) and the microwave (where most images are dominated by specular reflections), complex images with strong angular orientation effects and large dynamic ranges result.

3. If an imager is to be generally useful and not require optimally angled targets, it will be necessary to make use of the large signal margin that can be obtained with active systems.

4. One approach uses logarithmic signal processing and display to obtain detailed target signature information independent of target angular orientation.

5. Another approach simply divides the illumination power among a number of illumination angles (modes). While this reduces the illumination temperature in each mode, the temperature is still large in comparison to the noise temperature of the receivers.

6. It is shown that indirect lighting schemes, similar to those commonly used in the visible region, are attractive and can provide substantial signal margins while significantly mitigating glint and other specular effects that often dominate active images. It is also shown that this approach eliminates the need for strategically oriented targets.

7. Passive systems, while not having the large dynamic range of active systems, are inherently multimode and this, to some degree, compensates for their smaller dynamic range.

REFERENCES

1. R. Appleby and H. B. Wallace, "Standoff detection of weapons and contraband in the 100 GHz to 1 THz region," IEEE Trans. Antennas Propag. **55**, 2944–2956 (2007).
2. R. Appleby and D. A. Wikner, eds., *Passive Millimeter-Wave Imaging Technology X*, Proc. SPIE **6548** (2007).
3. D. L. Woolard, R. J. Hwu, M. J. Rosker, and J. O. Jensen, eds., *Terahertz for Military and Security Applications IV*, Proc. SPIE **6212** (2006).
4. R. Trebits, J. L. Kurtz, R. Appleby, N. A. Salmon, and D. A. Wikner, eds., *Radar Sensor Technology VIII and Passive Millimeter-Wave Imaging Technology VII*, Proc. SPIE **5410** (2004).
5. S. M. Kulpa and E. A. Brown, "Near-millimeter wave technology base study," HDL-SR-79-8 (Harry Diamond Laboratories, 1979).
6. G. A. Tanton, ed., *Millimeter Optics*, Proc. SPIE 259 (1980).
7. P. W. Kruse, "Why the military interest in near-millimeter wave imaging?" Proc. SPIE **259**, 94–97 (1980).
8. B. B. Hu and M. C. Nuss, "Imaging with terahertz waves," Opt. Lett. **20**, 1716–1718 (1995).
9. K. Wynne and D. A. Jaroszynski, "Superluminal terahertz pulses," Opt. Lett. **24**, 25–27 (1999).
10. Q. Chen, Z. Jiang, G. X. Xu, and X.-C. Zhang, "Near-field terahertz imaging with a dynamic aperture," Opt. Lett. **25**, 1122–1124 (2000).
11. J. O'Hara and D. Grischkowsky, "Quasi-optic synthetic phased-array terahertz imaging," J. Opt. Soc. Am. **B21**, 1178–1191 (2004).
12. D. N. Bittner, R. L. Crownover, F. C. De Lucia, and S. L. Shostak, "Passive imaging with a broadband cooled detector," *12th International Conference on Infrared and Millimeter Waves* (1987).
13. D. T. Petkie, F. C. De Lucia, C. Casto, and P. Helminger, "Active and passive millimeter- and sub-millimeter-wave imaging," Technologies for Optical Countermeasures II, Femtosecond Phenomena II, and Passive Millimetre-Wave and Terahertz Imaging II, Proc. SPIE **5989**, 598918 (2005).
14. E. N. Grossman, A. Luukanen, and A. J. Miller, "Terahertz active direct detection imagers," Terahertz for Military and Security Applications II, Proc. SPIE **5411**, 68–77 (2004).
15. F. B. Foote, E. E. Reber, and D. T. Hodges, "Active/passive near-millimeter wave imaging for tactical applications," Millimeter Optics, Proc. SPIE **259**, 131–136 (1980).
16. A. Bandyopadhyay, A. Stepanov, B. Schulkin, M. D. Federici, A. Sengupta, R. Barat, Z.-H. Michalopoulou, and D. Zimdars, "Terahertz interferometeric and synthetic aperture imaging," J. Opt. Soc. Am. **A23**, 1168–1178 (2006).
17. C. C. Aleksoff, "Synthetic-aperture techniques at near-millimeter wavelengths," Millimeter Optics, Proc. SPIE **259**, 115–124 (1980).
18. N. A. Salmon and R. Appleby, "Sky radiation temperature changes and fluctuations in the millimeter-wave band," Passive Millimeter-Wave Imaging Technology IV, Proc. SPIE **4032**, 98–102 (2000).
19. P. Bhartia and I. J. Bahl, *Millimeter Wave Engineering and Applications* (Wiley, 1984).
20. L. Yujiri, M. Shoucri, and P. Moffa, "Passive millimeter-wave imaging," IEEE Microwave Magazine (2003), pp. 39–50.